THE ASTROPHYSICAL JOURNAL, 417:663–670, 1993 November 10

A FAR-ULTRAVIOLET STUDY OF THE CYGNUS LOOP USING THE *VOYAGER* ULTRAVIOLET SPECTROMETERS

OLAF VANCURA,[1,2] WILLIAM P. BLAIR,[2,3] KNOX S. LONG,[2,3,4] JOHN C. RAYMOND,[1] AND J. B. HOLBERG[5]
Received 1993 February 24; accepted 1993 May 14

ABSTRACT

We have used the *Voyager 1* and *2* Ultraviolet Spectrometers to study the far-ultraviolet emissions from different types of shock waves in the Cygnus Loop. In the southeast and northern parts of the supernova remnant (SNR), we have measured the O VI λ1035 surface brightness from the main blast wave. This value is several times below the average and more than one order of magnitude below the peak O VI brightness in the SNR as measured with *Voyager*. A simple blast wave model appears able to reproduce the observations in the southeast and the northern parts of the Cygnus Loop but can only account for 10%–15% of the total O VI emission from the Cygnus Loop. The brightest O VI and C III λ977 emission is found coincident with optical filamentation and X-ray enhancements in the northeast. We interpret the observations in the northeast in terms of nonradiative and incomplete shocks whose surface area rises in the optical filamentary regions. We conclude that the bulk of the O VI emission from the Cygnus Loop arises from optically bright clouds within which intermediate-velocity (200 ± 50 km s^{-1}) nonradiative and incomplete shocks are widespread.

Subject headings: ISM: individual (Cygnus Loop) — radiation mechanism: miscellaneous — shock waves — supernova remnants — ultraviolet: interstellar

1. INTRODUCTION

With an angular extent of 3° × 4°, the Cygnus Loop offers astronomers a unique laboratory for studying a supernova remnant (SNR) on both the largest scale of global evolution and the microcosm of individual shock wave encounters with interstellar clouds. At an age of ~20,000 yr (Ku et al. 1984), the SNR is nearing the end of the adiabatic expansion phase. The Cygnus Loop is generally considered to be at a distance of 770 pc (Fesen, Blair, & Kirshner 1982; Hester, Raymond, & Danielson 1986), making the size of the remnant roughly 40 × 54 pc. Low reddening of $E(B-V) = 0.08$ (Miller 1974; Fesen et al. 1982) makes the Cygnus Loop ideal for study at nearly all energies, including the far-ultraviolet (FUV).

The Cygnus Loop shows a limb-brightened morphology at X-ray, optical, infrared (IR), and radio wavelengths (Ku et al. 1984; Fesen et al. 1982; Arendt, Dwek, & Leisawitz 1992; Keen et al. 1973). In the northeast part of the Cygnus Loop, X-ray emission extends from the bright optical filaments radially outward to faint Balmer-dominated filaments which demarcate the position of the main blast wave (see Chevalier, Kirshner, & Raymond 1980; Raymond et al. 1983; Hester et al. 1986; Long et al. 1992). In new imaging the Balmer-dominated emission may be traced not only in the northern third of the SNR but also over much of the eastern and western limbs (Fesen, Kwitter, & Downes 1992; Hanson & Winkler 1992; Winkler et al. 1993).

Observations over a wide range of energies are necessary to sample SNR shock waves in different components of the interstellar medium (ISM). The blast wave travels quickly through the intercloud medium (ICM) and heats this gas to millions of degrees. Secondary shocks are driven into clouds encountered by the primary shock. Within the clouds, higher preshock densities result in lower shock velocities and smaller cooling times. Thus, these intracloud shocks can emit profusely at UV, optical, and IR wavelengths while the primary shock continues to produce X-rays. In the Cygnus Loop, X-ray observations (Ku et al. 1984) yield a blast wave velocity ~400 km s^{-1}, while most UV and optical data are interpreted in terms of shock speeds ~100 km s^{-1} (see Raymond 1979; Raymond et al. 1980, 1981; Dopita et al. 1984).

FUV observations are critical to the complete understanding of SNRs because they bridge important gaps in the range of spectral energies, shock velocities, and shock types. Optical emission in SNRs arises predominantly in the recombination zone of radiative shocks, while the FUV emerges from hotter regions further upstream. FUV studies are also important for nonradiative shocks which have little or no recombination zone. These nonradiative shock waves (Raymond et al. 1983; Long et al. 1992) have velocities ~180 km s^{-1} in the Cygnus Loop and are prodigious emitters of O VI λ1035. O VI is a crucial diagnostic because its emissivity peaks near 300,000 K in ionization equilibrium, so it serves as a tracer of gas with temperatures between the X-ray gas (~10^6 K) and the gas sampled by other UV and optical lines ($\leq 10^5$ K). As such, the shocks which produce copious O VI have velocities intermediate to slower radiative shocks and the main blast wave (~160–300 km s^{-1}).

The first studies of the 900–1200 Å emission line spectra of SNRs were carried out by Shemansky, Sandel, & Broadfoot (1979), who used the *Voyager* Ultraviolet Spectrometers (UVSs) to study three isolated spatial regions in the Cygnus Loop. The spectra they obtained had strong lines at λ980 and λ1035, which they identified with C III λ977 and C II λ1035.

[1] Harvard-Smithsonian Center for Astrophysics, 60 Garden Street, Cambridge, MA 02138.
[2] Guest Observer with the *Voyager* Ultraviolet Spectrometers.
[3] Center for Astrophysical Sciences, Department of Physics and Astronomy, The Johns Hopkins University, 34th and Charles Streets, Baltimore, MD 21218.
[4] Space Telescope Science Institute, 3700 San Martin Drive, Baltimore, MD 21218.
[5] Lunar and Planetary Laboratory, University of Arizona, Tucson, AZ 85721.

Subsequently, Blair et al. (1991b, hereafter BLVH) used UVS data of the Cygnus Loop to construct the first FUV maps of any SNR. Although agreeing that Shemansky et al. (1979) had identified the λ980 line correctly, BLVH argued that the 1035 Å feature was O VI λλ1032, 1038, based on the morphology of the X-ray and optical images (and on line ratios).

More recently, the *Hopkins Ultraviolet Telescope* (*HUT*) was used to obtain 3.5 Å resolution spectra of two filaments in the Cygnus Loop. The observations conducted with *HUT* confirm that C III λ977 and O VI λλ1032, 1038 are the strongest lines between the Lyman limit and Lyα. Blair et al. (1991a) observed an incomplete radiative shock which shows strong O VI λ1035 in addition to moderate C III λ977 and N III λ991. Long et al. (1992) analyzed *HUT* data of a nonradiative filament in which O VI also dominated the sub-Lyα spectrum.

The purpose of the present study is to discuss large-scale FUV properties of the Cygnus Loop in more detail. We have obtained new observations of the Cygnus Loop with the *Voyager 1* and *2* UVSs. These data differ from the data of BLVH both in their coverage and in the orientation of the large UVS field of view. The new observations represent an attempt to isolate emissions from various components of the ISM. In particular, the data presented herein sample emissions from the main blast wave in the N and SE (directional abbreviations refer to the Cygnus Loop throughout), with coverage chosen to optimize the position angle to the *Voyager* slits with respect to the edge of the SNR. Also, the new data allow FUV analysis of discrete, adjoining spatial regions in the NE dominated optically either by nonradiative or radiative shocks. We present the observations and reductions in § 2, followed by an analysis and discussion of the implications in § 3. We briefly summarize in § 4.

2. OBSERVATIONS AND REDUCTIONS

2.1. *Voyager*

The *Voyager 1* and *2* UVSs are virtually identical objective grating spectrometers that are part of the instrumentation on board the *Voyager* spacecrafts, which have flown by many of the outer planets. During the "cruise" phase between and beyond the planets, these spectrometers have been used to observe a number of astronomical sources. As described by Broadfoot et al. (1977, 1981), each UVS employs a microchannel plate intensifier and 126 channel self-scanned array detector to sample the wavelength range between 500 and 1700 Å with a dispersion of 9.26 Å per channel. The field of view (FOV) is 0°.10 × 0°.87 projected on the sky, and the resolution for extended sources that fill the cross-dispersion direction of the FOV is ~38 Å. Although the large FOV prevents the detailed study of individual filaments in SNRs, it is acceptable for the study of large-scale structures in an extended object such as the Cygnus Loop.

We have obtained UVS spectra of three regions in the Cygnus Loop (see Fig. 1 and Table 1). In January–February

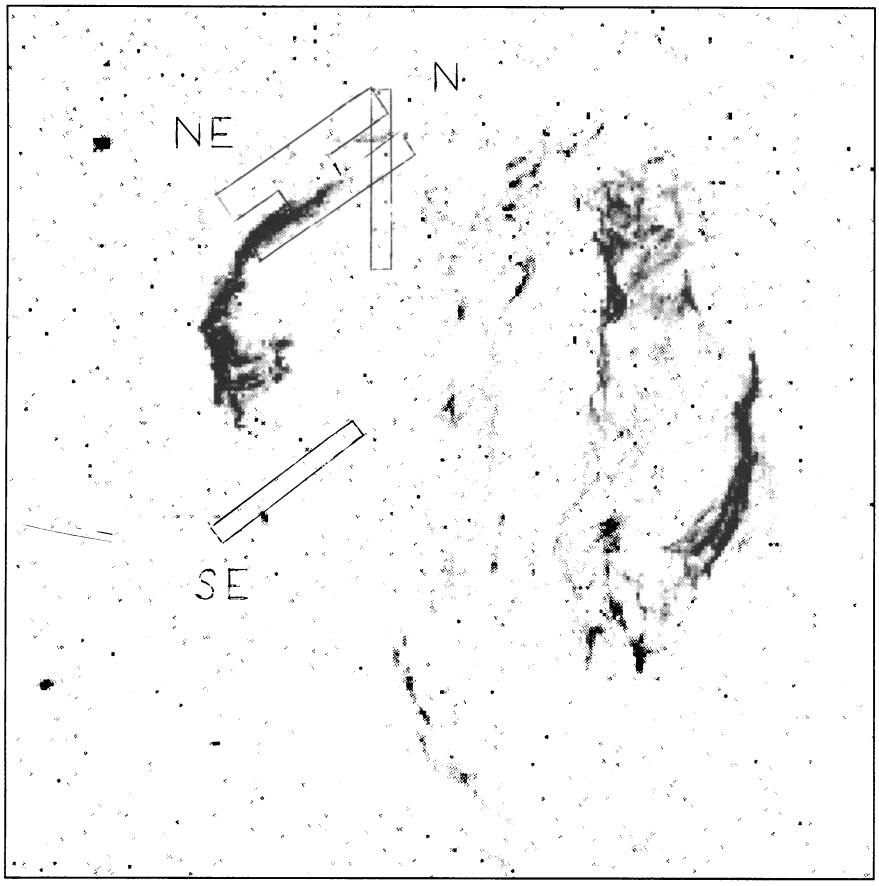

FIG. 1.—The Cygnus Loop in the light of [O III] λ5007. Overlaid are approximate aperture sizes (0°.1 × 0°.87), orientations, and locations for the observations in the NE and SE by *Voyager 2* and in the N by *Voyager 1*. The north and southeast regions had actual coverage extending ±0°.5 from the positions shown along the long axis of the aperture. The northeast *Voyager 2* data had the same position angle as the southeast data. For the northeast data, we show the total field coverage as defined by the motion of the center of the aperture.

TABLE 1

LOG OF *VOYAGER* OBSERVATIONS[a]

OBSERVATION	REGION OBSERVED α(1950)	REGION OBSERVED δ(1950)	INITIAL DATE	DURATION (hr)	NUMBER OF NEBULAR POINTINGS
V2–NE.....	313.0–314.0	31.3–32.1	1988 Jan 4	767	11
V1–N.....	313.0–313.3	31.2–32.6	1991 Apr 29	125	8
V2–SE.....	313.5–314.7	29.6–30.3	1991 June 19	276	8

[a] Background pointings not included. Background spectra were obtained in regions immediately outside the Cygnus Loop.

In Tables 1 and 2, *V1* and *V2* stand for *Voyager 1* and *Voyager 2*, respectively.

1988, we observed the northeast limb of the remnant with the *Voyager 2* FOV at a position angle of 130° east of north, nearly parallel to the X-ray shell and leading Balmer filaments. The region covered by this observation included not only the limb of the SNR but also extended in from the edge of the SNR to include the bright optical filaments in the northeast. In April–May 1991, we observed the northern limb of the Cygnus Loop with the *Voyager 1* FOV oriented in a north-south direction, nearly perpendicular to the periphery of the SNR. The region covered during this observation was selected to avoid the brightest optical emission in the north. In June–July 1991, we observed the southeast limb of the Cygnus Loop, with the *Voyager 2* FOV at a position angle of 130°, again perpendicular to the shock front. In this case the region covered also extended well outside the blast wave as defined by X-ray contours (Ku et al. 1984).

For each of these sets of observations, we achieved spatial coverage through a series of nominal pointings and ensuing spacecraft limit cycle motions as described in BLVH. Integration times in the NE, N, and SE were 767, 125, and 276 hr, respectively (see Table 1). Attitude control system error signals were used to reconstruct the pointing location for each spectrum as a function of time, and the data were binned on a 0°.01 × 0°.01 grid, with each spectrum placed into the grid point containing the center of the FOV. Emission maps were created by writing code that, for each normalized spatial grid point, calculated the total number of counts in specified UVS channels (47–51 for the 980 Å feature and 56–60 for the 1035 Å feature). This procedure is described in BLVH, which should be consulted for further details. Several instrumental corrections were applied in the reduction of the UVS data. These standard corrections, which are described by Holberg (1986, 1991), include "fixed pattern noise" flat fielding, dark and sky background subtraction, and a correction for instrumental scattering. Finally, a time-dependent sky background template spectrum was scaled to each individual Cygnus Loop spectrum and subtracted.

Like the global spectrum obtained by BLVH, the average spectrum of the NE region (Fig. 2) shows strong features at λ980 and λ1035, and we identify these as C III λ977 and O VI λλ1032, 1038, respectively. Using various tasks in IRAF[6], we have measured the fluxes in these features, which we present in Table 2. The reddening correction was accomplished using the Seaton (1979) Galactic extinction curve.

[6] IRAF is distributed by the National Optical Astronomy Observatories, which is operated by the Association of Universities for Research in Astronomy (AURA), Inc. under cooperative agreement with the National Science Foundation.

Because the UVS has no spatial resolution, the images we have constructed of the northeast show little structure along the long axis of the FOV (Vancura 1992). However, both the C III and O VI emissions gradually increase in brightness (we will refer to this location as region I) toward the center of the remnant, finally reaching a plateau (region P). This effect may be seen in sample spectra of each of these two regions (Fig. 3) and in their emissions (Table 2). (There is roughly an 8 Å redshift in the spectrum of region I which occurs because the aperture is not uniformly illuminated with emission. The shift is consistent in sense and magnitude with the gradient in flux entering the aperture.) The surface brightness in region P is several times the average from the global data of BLVH and is in fact brighter than any region in our earlier FUV maps of the Cygnus Loop. This presumably is an effect of the aperture orientation and larger filling factor of emission in the 1988 data.

For the blast wave observations, comparison with the X-ray primary shock location reveals that at each observed position we detect very faint λ1035 emission in the post–blast wave gas only. In the southeast, the λ1035 emission appears spatially uniform; however, the low signal-to-noise ratio prevents a definitive analysis of any spatial variations. We present the observed average postshock spectrum in the southeast in Figure 4, in which there may be some evidence for weak C III λ977 emission. In Figure 5, we present the post–blast-wave spectrum obtained of the northern X-ray shock front. The λ1035 feature is clearly stronger than any λ977 feature, but as was the case in the southeast, we have detected emission in the post–blast-wave gas only. The signal-to-noise ratio is low and no spatial structure is observed in either the λ977 or λ1035 map. The measured brightness of O VI (see Table 2) is a factor of 2 higher than in the southeast.

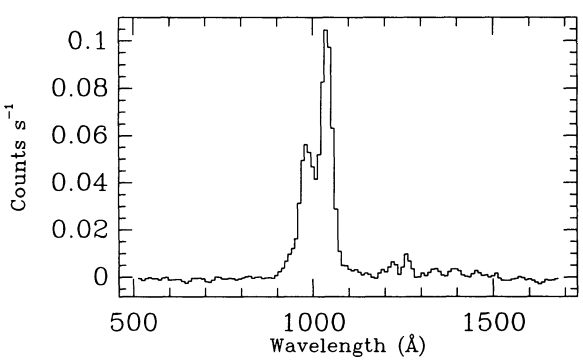

FIG. 2.—Average spectrum of the northeast region as sampled by *Voyager 2*. The apparent Lyα feature is an artifact of the reduction procedure.

TABLE 2

VOYAGER OBSERVED AND DEREDDENED SURFACE BRIGHTNESSES[a]

	Emission Feature			
	C III λ977		O VI λ1035	
Parameter	$F(\lambda)$	$I(\lambda)$	$F(\lambda)$	$I(\lambda)$
Global average[b]	4.0	12	8.8	22
V2–SE	0.2	0.6	1.1	2.8
V1–N	...	...	2.2	5.6
V2–I	3.2	9.4	11	30
V2–P	16	48	35	90

[a] Reddening correction assumes an extrapolated Seaton (1979) curve and $E(B-V) = 0.08$. All surface brightnesses are given in units of 10^{-6} ergs cm^{-2} s^{-1} sr^{-1}.

[b] Global values taken from Blair et al. (1991b).

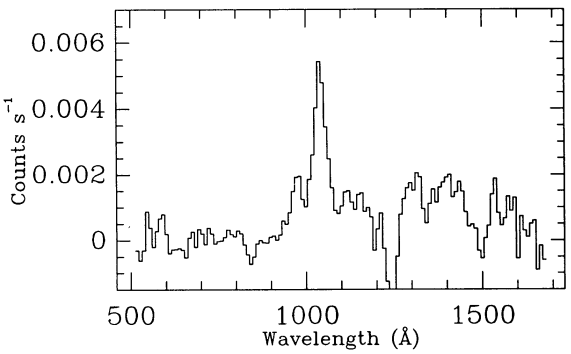

FIG. 4.—Spectrum of the post–blast-wave region in the southeast as sampled by *Voyager 2*. Although O VI λ1035 is detected, the brightness is roughly a factor of 8 below the global average of Blair et al. (1991b). There is evidence for weak C III λ977.

2.2. *X-ray and Optical Flux Distributions in the NE*

The size of the *Voyager* FOV complicates interpretation of the data, so to address the nature of the *Voyager* emissions in the NE in more detail, we have sampled additional maps (at other wavelengths) in the manner of *Voyager*. X-ray data used were the *Einstein* IPC map (Ku et al. 1984) as reprocessed by Seward (1990), while an Hα image of the NE Cygus Loop was provided by Winkler et al. (1993). On the large scale of the *Voyager* FOV, the *bright* emission in the Hα image is essentially identical to [O III] emission in the northeast region. However, the Hα image is also deep enough to show the faint nonradiative Balmer-dominated shocks associated with the main blast wave. Bright stars in the optical image were removed using tasks in IRAF. Beginning with the Hα image, we also have used IRAF tasks to remove most of the bright optical stellar and SNR emission, leaving as SNR emission only the nonradiative Balmer shocks and faint emission circumscribing the bright optical filaments. We shall refer to this image as the "Balmer" image. Although there are still faint residual images of stars in the Hα pictures, they are relatively homogeneous and contribute little more than a pedestal in the background level of the convolved maps. In each case, this pedestal level was determined from regions outside the SNR and subtracted.

We have written computer programs to pass a *Voyager*-like false aperture at the appropriate position angle over these comparison data to sample them as if observed by *Voyager* (see BLVH). In each case, our binning scheme and the time-sampling drop-outs were duplicated in the *Voyager*-convolved images. As was the case with the *Voyager* O VI and C III images of the northeast, the convolved comparison northeast images show very little structure in the spatial direction parallel to the long axis of the FOV (Vancura 1992). Using a slit width of 0°.1, we have thus averaged each of the NE *Voyager* images (observed and comparison) along the long axis to create one-dimensional cross cuts of this region, presented in

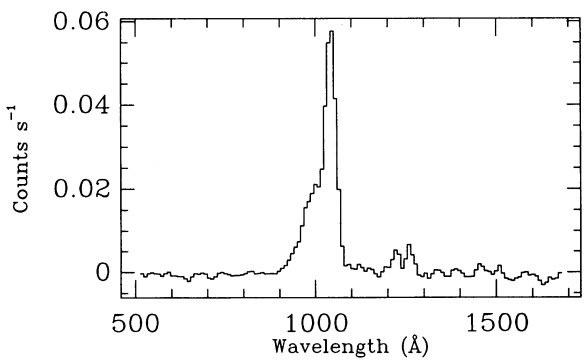

FIG. 3*a*

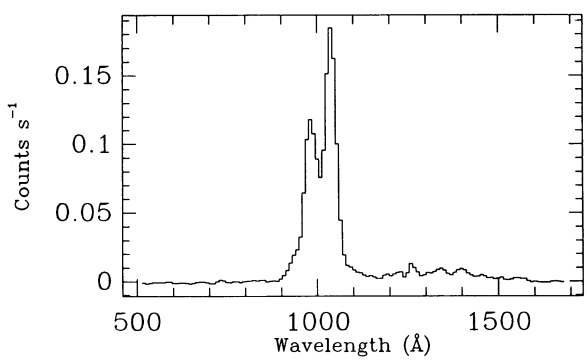

FIG. 3*b*

FIG. 3.—Sample spectra of (*a*) region I, and (*b*) region P in the northeast.

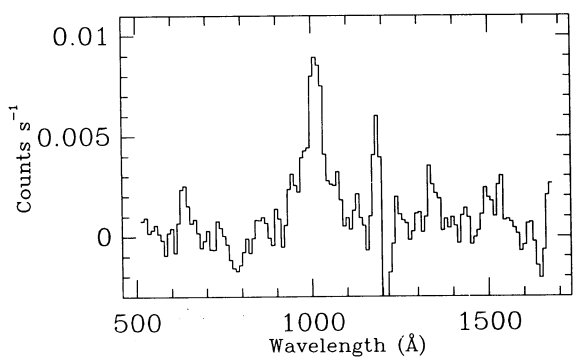

FIG. 5.—Spectrum of the post–blast-wave region in the N as sampled by *Voyager 1*. O VI is detected at a level roughly twice that of Fig. 4 but still significantly below the average global spectrum of Blair et al. (1991b). C III is not present at a detectable level.

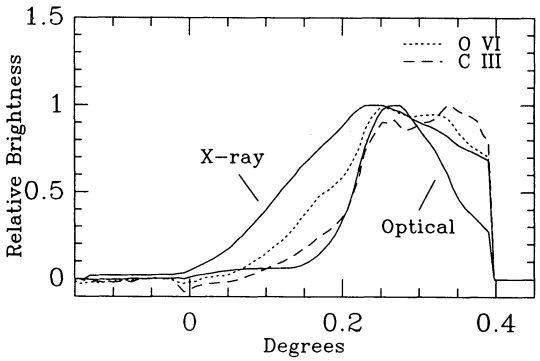

FIG. 6a

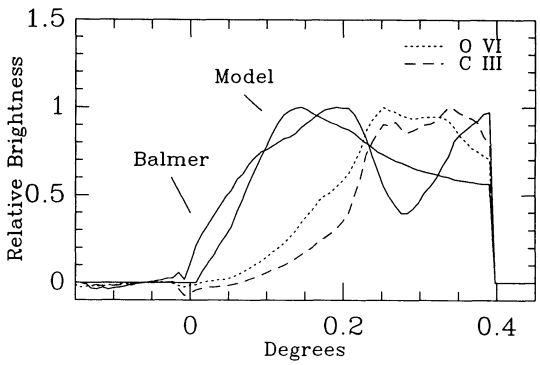

FIG. 6b

FIG. 6.—One-dimensional representation of the NE maps. The x-axis is in degrees, with zero taken to be the X-ray shock front and positive angles corresponding to radially inward. The y-axis is relative intensity in arbitrary units. In (*a*) the dashed and dotted curves represent C III and O VI, respectively, while the solid curves correspond to X-ray and optical emission. Panel (*b*) is the same as (*a*), except that the Balmer and model blast wave emissions are plotted as solid curves.

Figure 6. In each panel, the dashed curve represents C III emission and the dotted curve, O VI. The positive x-axis corresponds to the inward radial direction, and the zero point is taken to lie at the X-ray shock front. Region I corresponds to the region roughly between 0°.0 and 0°.22, with region P from 0°.22 to 0°.4. Overlaid on Figure 6*a* are the X-ray and optical data sampled in the same manner. It is clear that the optical data provide a good match to the plateau, with the X-ray emission being more extended but also a reasonable match. In Figure 6*b*, we show for comparison the Balmer image sampled in the same one-dimensional manner. Clearly, the Balmer convolution does not reproduce the observed distribution of O VI and C III.

3. ANALYSIS AND DISCUSSION

The *HUT* observations of two filaments in the Cygnus Loop have permitted unambiguous identifications of the strong λ977 and λ1035 emission features in our *Voyager* spectra. The incomplete radiative shock observed by Blair et al. (1991a) shows a strong, clearly resolved O VI doublet at $\lambda\lambda$1032, 1038. Additionally, the sub-Lyα portion of the spectrum shows C III λ977 and N III λ991 at observed flux levels which are 31% and 20% of O VI, respectively. Aside from airglow lines, there are no other sub-Lyα lines detected. Long et al. (1992) report *HUT* data of a nonradiative filament in the northeast Cygnus Loop first studied by Raymond et al. (1983). Despite the presence of very strong O VI emission, N III was not detected (although it should be noted that an airglow line near N III might make a weak feature difficult to detect).

We therefore ascribe the λ980 feature in the *Voyager* spectra primarily to C III λ977 and the λ1035 feature to O VI $\lambda\lambda$1032, 1038. Even if there is a small contribution from N III λ991, its effect will not compromise any of the conclusions we reach below. The ionization potential for N^{+2} is similar to that for C^{+2}, and the excitation energies are about equal. Thus, we would expect any N III λ991 emission to have a very similar distribution to C III λ977 (and optical lines). (Note: In deriving fluxes from the various spectra we have obtained, we have considered spectral fits which included N III as well as C III and O VI, but in all cases the additional degree of freedom was not justified.) Additionally, radiative shock models (see Hartigan, Raymond, & Hartmann 1987) indicate N III:C III ratios of 0.3 for velocities near 160 km s^{-1} and much less otherwise.

3.1. *Emission from the Primary Shock Front*

The fluxes of O VI that we observe in the SE, N, and on the NE rim (*Voyager 2*, region I) are 2.8, 5.6, and 30 $\times$ 10^{-6} ergs cm^{-2} s^{-1} sr^{-1}, respectively. We would like to know to what degree the fluxes we have measured in these regions can be attributed to the X-ray shock front. In order to make this comparison, we have constructed models of the spectrum expected from a spherical blast wave centered at α: $20^h49^m15^s$, δ: 30°51′30″, radius of 84′, preshock density of 0.15 cm^{-3} (Ku et al. 1984), and distance of 770 pc. We have used Raymond's (1979) code with modifications as discussed in Cox & Raymond (1985) and have assumed abundances appropriate for the Cygnus Loop (see Long et al. 1992). For these conditions, most of the nonradiative O VI emission arises within 0.6 pc of the shock front. Our model predicts a face-on surface brightness (from a single shock) in O VI of 6.3 $\times$ 10^{-7} ergs cm^{-2} s^{-1} sr^{-1} after 2000 yr. Truncating the shock at 20,000 yr increases the surface brightness slightly to 7.7 $\times$ 10^{-7} ergs cm^{-2} s^{-1} sr^{-1}. Predicted brightnesses of C III and N III from the single shock are 6.2 $\times$ 10^{-8} ergs cm^{-2} s^{-1} sr^{-1} and 4.2 $\times$ 10^{-9} ergs cm^{-2} s^{-1} sr^{-1}, respectively, which are independent of the cutoff age, since the postshock gas is ionized quickly beyond C^{+2} and N^{+2}.

To compare the blast wave model predictions with the data, the *Voyager* aperture orientation must be taken into account. since the FOV is projected onto a spherical geometry. Analytically, we find geometric correction factors of 3.8 in the southeast and north and 10.0 in the northeast (a result of the fact that the slit is parallel to the shock front in the northeast). Thus, for the spectra in the north and southeast, the predicted fluxes are each about 2.7 $\times$ 10^{-6} ergs cm^{-2} s^{-1} sr^{-1}, while the predicted flux in the northeast is about 7.0 $\times$ 10^{-6} ergs cm^{-2} s^{-1} sr^{-1}.

We therefore conclude that in the SE Cygnus Loop, the observed O VI emission can be accounted for by this simple blast-wave model. However, the brightness of O VI in the SE region in only $\frac{1}{8}$ of the observed average for the entire SNR. Thus, even if our model blast wave covers the surface of a sphere of radius 19 pc, we can reproduce only 10%–15% of the total O VI luminosity. The factor of 2 difference in observed O VI brightness between the north and southeast may be due to density variations between the two regions. The spatially averaged X-ray emission in the north is twice as bright as in the

southeast (Ku et al. 1984) and suggests a higher preshock density in the north. The increased brightness of the Balmer filaments in the north relative to the SE (see Hester et al. 1986; Fesen et al. 1992; Hanson & Winkler 1992; Winkler et al. 1993) also suggests higher preshock densities or a greater surface area of intermediate velocity shocks, although a higher preshock neutral fraction may also be responsible. Finally, the northeast limb requires even higher preshock densities than in the southeast or north.

3.2. *A Detailed Look at the NE Region*

We turn now to an analysis of the *Voyager* observations in the NE and the interrelation between FUV, optical, and X-ray emissions there. The surface brightness distribution expected from a spherical blast wave in the northeast as described above, summed in the same one-dimensional manner, is shown in Figure 6*b*. For the northeast data, inspection of Figure 6 reveals that the convolved optical data and X-ray data best match the morphology of the FUV plateau, while the convolved versions of the Balmer image and blast wave model clearly fail, since they each predict too much emission near the primary shock. The X-ray enhancement coincident with the bright optical filaments in the northeast may be understood by appealing to reverse shocks in the post–blast-wave flow (see McKee & Ostriker 1977; Hester & Cox 1986), within which the shocked cloud emits optically while the overpressured region produces enhanced X-ray emission. Thus, in the plateau region, the O VI and C III emissions are spatially associated with the bright optical filaments. The spatial correlation between C III and optically emitting shocks is as expected; however, the association of O VI with the optical emission merits further discussion.

Rasmussen & Martin (1992), using sounding-rocket data of the Cygnus Loop, have recently shown evidence for bulk motions of 185 km s^{-1} in O VI, suggesting a shock wave origin. For this to be true in the optically emitting regions in the northeast, variations in density and shocked velocity are required in the eastern clouds, but this appears quite reasonable. In light of the X-ray observations of Ku et al. (1984), ram pressure (ρv^2) equilibrium between the primary and secondary shock waves dictates that shocks in excess of 160 km s^{-1} have preshock densities of a few atoms per cubic centimeter. If the preshock densities are much greater than this, velocities will be too small to produce O VI. Raymond et al. (1988), in studying the filament known as the "spur," found evidence for shock velocity variation between 80 km s^{-1} in the NW and 140 km s^{-1} in the south east for this single filament, and concluded that the data were consistent with emission from a cloud of radially decreasing density. As further suggested by our *Voyager* data, the eastern filamentary structure in the Cygnus Loop thus appears to contain shocks with a wide range of velocities and preshock densities. Clouds presumably have some sort of density fall-off between the cloud cores and the intercloud medium while maintaining pressure equilibrium among the various components. The shocks driven into the intermediate density component are responsible for the bulk of the O VI production.

In the optical filamentation, the filling factor of shock waves with velocities ≥ 160 km s^{-1} must be large. For a bright optical filament in the eastern Cygnus Loop, Blair et al. (1991a) found a shock velocity of ~ 170 km s^{-1} and reported a surface brightness of 1.0×10^{-4} ergs cm^{-2} s^{-1} sr^{-1} in O VI. The present observation of the plateau yields a surface brightness of 3.5×10^{-5} ergs cm^{-2} s^{-1} sr^{-1} in O VI, even though the *Voyager* FOV is not completely filled.

The picture outlined above is especially appealing if the clouds in the east are presently being struck by the main blast wave as Hester & Cox (1986) have suggested and the data of Raymond et al. (1988) and Teske (1990) support. A blast wave presently making its way into and around large clouds continuously produces O VI from shock waves driven into the intermediate density component. Thus, slow and intermediate velocity shocks emit in sheets which mimic the spatial extent of the clouds. In this picture the appearance of the bright optical filaments "behind" the eastern edge of the remnant (as defined by the X-ray emission and the Balmer filaments) is simply a projection effect.

We may obtain an estimate of the number of shocks filling the FOV as follows. Assuming ram pressure equilibrium and complete recombination to O^{+4}, our modeling indicates that shock waves with velocities ranging from 200–220 km s^{-1} will emit the most O VI. We adopt a preshock density of 2 cm^{-3}, consistent with preshock densities obtained in Long et al. (1992) and Hester, Raymond, & Blair (1993), and pressure equilibrium between the blast wave and O VI emitting shocks. A 200 km s^{-1} shock will have a face-on surface brightness of 1.7×10^{-4} ergs cm^{-2} s^{-1} sr^{-1} in O VI after roughly 1400 yr, at which point O VI production ceases. Truncating the shock at 250 yr reduces the O VI emission by a factor of 4. If we assume that the FOV is filled with face-on shocks of 200 km s^{-1} at an age of 250 yr, then the number of shocks along the line of sight, N, necessary to reproduce the O VI emission of the plateau region (see Table 2) is of order unity. If multivelocity shocks are present, or if the preshock density is less than 2 cm^{-3}, N is necessarily higher. On the other hand, if the timescale for evolution is greater, if we are seeing shocks at an oblique angle, or if the preshock density is higher, then N may be less. We estimate these effects to lead to an order of magnitude uncertainty in N.

In region I, the region out in front of the bright optical filaments, the brightness of O VI suggests considerable density enhancement compared to the southeast or north. Copious O VI from nonradiative shocks ($V \sim 175$ km s^{-1}) has been predicted (Raymond et al. 1983) and observed with *HUT* (Long et al. 1992). Comparison with the convolved Balmer map (Fig. 6*b*) shows that there is considerable nonradiative shock emission spatially coincident with region I. We emphasize that the similarity with the Balmer image will not be perfect. Balmer filaments only appear if the shocks are encountering partly neutral preshock material, so that the postshock H has some probability of being excited before being ionized (cf. Chevalier et al. 1980). Raymond et al. (1983) and Long et al. (1992) suggest that it is reasonable to assume that roughly 30% of the preshock gas was neutral in a filament selected on the basis of its bright Hα emission. Hester & Raymond (1987) and Hester et al. (1993) demonstrate that there are portions of many Balmer filaments in the NE which are beginning to emit [O III] $\lambda\lambda$4959, 5007 and appear to be in transition to becoming radiative. They suggest that shocks complete to O^{+2} have sufficient UV precursor emission to completely preionize hydrogen. In this case there would be no associated Balmer line emission from the shock, but copious O VI production could continue.

The C III:O VI ratio in region I (see Table 2) appears much too strong for nonradiative shocks or shocks complete to O^{+5} to be the sole source of emission. At the peak ionization struc-

ture behind a 180 km s^{-1} shock, there is no C^{+2}. Thus, as the age of these shocks increases, very large column depths (hence, fluxes) of O VI can be built up while the emission in C III, coming only from the ionizing shock front itself, remains constant at a relatively small value. Balmer filaments in transition to becoming radiative, of the kind reported in the northeast by Hester & Raymond (1987), are probably responsible for the enhancement of C III above that expected from this picture. Because these filaments are emitting in [O III], we also expect some to yield C III emission, since the C^{+2} zone is near O^{+2} in the recombination flow. Mixing with these faint "transition" shocks can increase the strength of C III:O VI compared to nonradiative shocks alone.

To summarize, the northeast observations can be interpreted as follows. The different $\lambda 1035:\lambda 980$ ratios in the two spatial regions (see Fig. 3) argue for different velocities/types of shocks dominating the emissions in each region. In region I, the O VI flux comes primarily behind intermediate velocity nonradiative and incomplete radiative shocks ($\sim 200 \pm 50$ km s^{-1}) where the main blast wave of ~ 400 km s^{-1} has encountered density enhancements of a few. Some C III arises behind those intermediate velocity shocks which are complete at least to the C^{+2} zone of the recombination flow. The surface brightness for each line is proportional to the surface area of these shocks entering the *Voyager* FOV. Furthermore, these shocks are widespread even in the optical filamentary regions (region P), where the surface brightness of C III and O VI increase. Since the plateau region also samples the slower, optically bright radiative shocks, the C III:O VI ratio rises as expected. Assuming that the same types of shocks are responsible for O VI emission in the two regions, we find that roughly *half* the C III emission in the optically bright regions is emitted behind intermediate velocity shocks, the other half coming from slower (~ 100 km s^{-1}) radiative shocks. This further implies that much of the other intermediate ionization emission often attributed to slower shocks (e.g., O III] $\lambda 1663$, [O III] $\lambda\lambda 4959$, 5007) may instead arise in ~ 200 km s^{-1} shocks. As shocks above 150 km s^{-1} may be thermally unstable (see Innes 1992; Innes, Giddings, & Falle 1987), steady-state shock modeling may not be appropriate.

Rasmussen & Martin (1992) have suggested that the bulk motion of 185 km s^{-1} they observed in O VI arises primarily from a main blast wave presently moving at ~ 250 km s^{-1}. In fact, if cooling compresses the postshock flow by a further factor of 2–3, as appears to be the case in the *HUT* nonradiative filament (see Long et al. 1992), the implied shock velocity may be as low as 200 km s^{-1}. However, the notion that the bulk of the O VI emission from the Cygnus Loop arises from the main blast wave is clearly at odds with the *Voyager* data, which demonstrates that the brightest O VI is spatially associated with the optical filaments and that a blast wave morphology for the O VI emission is incompatible. Hester et al. (1993) argue that nonradiative filaments in the northeast are the result of the blast wave encountering a shell. The *Voyager* measurements of O VI surface brightness from the main blast wave in the SE suggest that in this region, the shell is either missing or has not yet been encountered.

4. CONCLUSIONS

We have used the *Voyager 1* and *2* UVSs to study the FUV emission from the Cygnus Loop. In spectra sampling the blast wave in the southeast and north, we find a surface brightness in O VI that is several times below the average and more than one order of magnitude below the peak observed brightness in the northeast. A simple blast-wave model with parameters determined from X-ray observations (Ku et al. 1984) appears able to reproduce the observed O VI emission in the SE. However, this blast wave can account for only 10%–15% of the total O VI emission from the remnant.

In the northeast Cygnus Loop with the *Voyager* aperture oriented parallel to the primary shock, we observe that the C III and O VI emissions both increase in brightness behind the primary shock toward the center of the remnant (region I) before leveling off to a plateau (region P). The surface brightness of O VI in region P is roughly four times the global average. Different ratios for O VI:C III in regions I and P suggest that different types of shocks are contributing to the emissions in each region.

The plateau constitutes the brightest O VI and C III emission detected in our data and is spatially coincident with the bright optical filaments and accompanying X-ray enhancement in the NE. We conclude that O VI producing shocks with velocities ≥ 160 km s^{-1} must be widespread in the optically bright regions. This is consistent with the main blast wave presently encountering intermediate density material at the cloud/ICM interface. Radially further outward in region I, the O VI and C III both come primarily from nonradiative and incomplete shocks. The O VI flux is less than in the optically bright regions because the filling factor of intermediate velocity (~ 200 km s^{-1}) shocks is less. The C III brightness is less for the same reason and because of the absence of slower, radiative shocks responsible for much of the bright eastern optical emission.

We are indebted to F. Winkler for providing us with a deep Hα CCD mosaic image of the NE Cygnus Loop prior to publication and F. Seward for providing the reprocessed X-ray data. We also thank J. Collins and H. Lutz for their valuable assistance in the reduction of a large portion of the *Voyager* data. Third project was supported by NASA grants NAG5-988 and NAG5-1276 to The Johns Hopkins University and NAG-528 to The Smithsonian Astrophysical Observatory.

REFERENCES

Arendt, R. G., Dwek, E., & Leisawitz, D. 1992, ApJ, 400, 562
Blair, W. P., et al. 1991a, ApJ, 379, L33
Blair, W. P., Long, K. S., Vancura, O., & Holberg, J. B. 1991b, ApJ, 374, 202 (BLVH)
Broadfoot, A. L., et al. 1977, Space Sci. Rev., 21, 183
———. 1981, J. Geophys. Res., 86, 8259
Chevalier, R. A., Kirshner, R. P., & Raymond, J. C. 1980, ApJ, 235, 186
Cox, D. P., & Raymond, J. C. 1985, ApJ, 298, 651
Dopita, M. A., Binette, L., D'Odorico, S., & Benvenuti, P. 1984, ApJ, 276, 653
Fesen, R. A., Blair, W. P., & Kirshner, R. P. 1982, ApJ, 262, 171
Fesen, R. A., Kwitter, K. B., & Downes, R. A. 1992, AJ, 104, 719
Hanson, G. J., & Winkler, P. F. 1992, BAAS, 24, 1231
Hartigan, P., Raymond, J., & Hartmann, L. 1987, ApJ, 316, 323
Hester, J. J., & Cox, D. P. 1986, ApJ, 300, 675
Hester, J. J., & Raymond, J. C. 1987, in IAU Colloq. 101, Supernova Remnants and the Interstellar Medium, ed. R. S. Roger & T. L. Landecker (Cambridge: Cambridge Univ. Press), 415
Hester, J. J., Raymond, J. C., & Blair, W. P. 1993, ApJ, submitted
Hester, J. J., Raymond, J. C., & Danielson, G. 1986, ApJ, 303, L17
Holberg, J. B. 1986, ApJ, 311, 969
———. 1991, in IAU Colloq. 123, Observations in Earth Orbit and Beyond, ed. Y. Kondo (Dordrecht: Kluwer), 49
Innes, D. E. 1992, A&A, 256, 660
Innes, D. E., Giddings, J. R., & Falle, S. A. E. G. 1987, MNRAS, 226, 67
Keen, N. J., Wilson, W. E., Haslam, C. G. T., Graham, D. A., & Thomasson, P. 1973, A&A, 28, 197

Ku, W. H.-M., Kahn, S. M., Pisarski, R., & Long, K. S. 1984, ApJ, 278, 615
Long, K. S., Blair, W. P., Vancura, O., Bowers, C. W., Davidsen, A. F., & Raymond, J. C. 1992, ApJ, 400, 214
McKee, C. F., & Ostriker, J. P. 1977, ApJ, 218, 148
Miller, J. M. 1974, ApJ, 189, 239
Rasmussen, A., & Martin, C. 1992, ApJ, 396, L103
Raymond, J. C. 1979, ApJS, 39, 1
Raymond, J. C., Black, J. H., Dupree, A. K., Hartmann, L., & Wolff, R. S. 1980, ApJ, 238, 881
———. 1981, ApJ, 246, 100
Raymond, J. C., Blair, W. P., Fesen, R. A., & Gull, T. R. 1983, ApJ, 275, 636
Raymond, J. C., Hester, J. J., Cox, D., Blair, W. P., Fesen, R. A., & Gull, T. R. 1988, ApJ, 324, 869
Seaton, M. J. 1979, MNRAS, 187, 73P
Seward, F. D. 1990, ApJS, 73, 781
Shemansky, D. E., Sandel, B. R., & Broadfoot, A. L. 1979, ApJ, 231, 35
Teske, R. G. 1990, ApJ, 365, 256
Vancura, O. 1992, Ph.D. thesis, The Johns Hopkins University
Winkler, P. F., et al. 1993, in preparation